

A CONDITIONAL LUMINOSITY FUNCTION MODEL OF THE COSMIC FAR-INFRARED BACKGROUND ANISOTROPY POWER SPECTRUM

FRANCESCO DE BERNARDIS, ASANTHA COORAY

Department of Physics and Astronomy, University of California, Irvine, CA 92697

Draft version November 9, 2018

ABSTRACT

The cosmic far-infrared background (CFIRB) is expected to be generated by faint, dusty star-forming galaxies during the peak epoch of galaxy formation. The anisotropy power spectrum of the CFIRB captures the spatial distribution of these galaxies in dark matter halos and the spatial distribution of dark matter halos in the large-scale structure. Existing halo models of CFIRB anisotropy power spectrum are either incomplete or lead to halo model parameters that are inconsistent with the galaxy distribution selected at other wavelengths. Here we present a conditional luminosity function approach to describe the far-IR bright galaxies. We model the 250 μm luminosity function and its evolution with redshift and model-fit the CFIRB power spectrum at 250 μm measured by the Herschel Space Observatory. We introduce a redshift dependent duty-cycle parameter so that we are able to estimate the typical duration of the dusty star formation process in the dark matter halos as a function of redshifts. We find the duty cycle of galaxies contributing to the far-IR background is 0.3 to 0.5 with a dusty star-formation phase lasting for $\sim 0.3 - 1.6$ Gyrs. This result confirms the general expectation that the far-IR background is dominated by star-forming galaxies in an extended phases, not bright starbursts that are driven by galaxy mergers and last $\sim 10 - 100$ Myrs. The halo occupation number for satellite galaxies has a power-law slope that is close to unity over $0 < z < 4$. We find that the minimum halo mass for dusty, star-forming galaxies with $L_{250} > 10^{10} L_{\odot}$ is $2 \times 10^{11} M_{\odot}$ and $3 \times 10^{10} M_{\odot}$ at $z = 1$ and 2 , respectively. Integrating over the galaxy population with $L_{250} > 10^9 L_{\odot}$, we find that the cosmic density of dust residing in the dusty, star-forming galaxies responsible for the background anisotropies $\Omega_{\text{dust}} \sim 3 \times 10^{-6}$ to 2×10^{-5} , relative to the critical density of the Universe.

1. INTRODUCTION

The total intensity of the cosmic far-infrared background (CFIRB) is now established with absolute photometry (Puget et al. 1996; Fixen et al. 1998; Dwek et al. 1998). This background originates from the UV and optical emission of young stars, absorbed by the dust in galaxies and then re-emitted in the infrared (IR) wavelengths. Deep surveys with instruments aboard the *Herschel* Space Observatory have started to resolve this background intensity between 100 and 500 μm to discrete galaxies based on resolved counts (Oliver et al. 2010; Clements et al. 2010; Berta et al. 2011). Unfortunately even the deepest images of the far-IR sky using PACS and SPIRE are limited by source confusion. For example, at 250, 350, and 500 μm , only 15, 10 and 6% of the total background intensity is resolved to individual galaxies, respectively. Instead of individual detections, the fainter galaxies responsible for the bulk of the CFIRB intensity is studied with statistics such as $P(D)$, the probability of deflections (Glenn et al. 2010), and $P(k)$, the angular power spectrum of CFIRB anisotropies resulting from the correlated confusion noise (Haiman & Knox 2000; Knox et al. 2001; Scott & White 1999; Negrello et al. 2007; Ambard & Cooray 2007).

While attempts were made to detect the power spectrum of CFIRB with *Spitzer*-MIPS at 160 μm (Lagache et al. 2007), and a limited low signal-to-noise ratio detection with BLAST (Devlin et al.

2009) in Viero et al. (2009), the first clear detection of the CFIRB anisotropy power spectrum from 30 arcseconds to 30 arcminute angular scales came from *Herschel*-SPIRE at 250, 350 and 500 μm (Amblard et al. 2011). This was soon followed by Planck measurements of the CFIRB power spectrum from 5 arcminute to degree angular scales (Planck Collaboration, 2011). At the longer mm-wavelengths, clustering of dusty galaxies can also be studied as part of the CMB secondary anisotropy studies, where a combination of signals contribute to the total power spectrum (Addison et al. 2011; Archidiacono et al. 2012). While the arcminute-scale ground-based CMB experiments and Planck can study the large-angular correlations in the CFIRB at linear scales, the angular resolution of *Herschel*-SPIRE (Griffin et al. 2010) is such that the measurements probe the non-linear scales and capture important information on how the dusty star-forming galaxies are distributed in the dark matter halos.

First predictions on the CFIRB anisotropy power spectrum concentrated on the linear power spectrum scaled by a bias factor (Scott & White 1999; Haiman & Knox 2000; Knox et al. 2001). Since those early studies a popular approach to describe the large-scale structure galaxy distribution is to connect galaxies to the underlying dark matter halo distribution (see review in Cooray & Sheth 2002). This halo modeling allows a way to describe the galaxy clustering power spectrum and correlation function through the halo occupation number describing the number

of galaxies in a given dark matter halo as a function of the halo mass. Recent improvements in the halo model involve an occupation number description that takes into account for the luminosity dependence of the satellites through what are now called conditional luminosity functions (CLFs; Yang et al. 2004; Cooray & Milosavljevic 2005; Cooray 2006a).

While an attempt was made to incorporate CLFs to describe the CFIRB power spectrum (Amblard & Cooray 2007; see recent works in Shang et al. 2011; Wang et al. 2011; Xia et al. 2012), this was based on a phenomenological model for the number counts and luminosity functions (LFs) of far-IR sources (Lagache et al. 2003). The number counts and LF measurements from the *Herschel* Space Observatory now allow us to both improve the model and extract parameters of the underlying CLF description.

Separately, modeling of recent measurements of the CFIRB anisotropy power spectrum with *Herschel* and Planck, and the dusty galaxy signal in CMB secondary anisotropy data, is somewhat controversial. The best-fit parameters of the original study (Amblard et al. 2011) either had a power-law slope for satellites that was steeper than 1.3 or had a relation between the satellite mass scale M_{sat} and the minimum halo mass to host a galaxy M_{min} such that $M_{\text{sat}} \sim (3 - 4)M_{\text{min}}$. The galaxy clustering measurements in the optical band show that the power-law slope is slightly less than 1 (Zehavi et al. 2004; Abazajian et al. 2005), while $M_{\text{sat}} \sim (15 - 20)M_{\text{min}}$ (Gao et al. 2004; Kravtsov et al. 2003; Zheng et al. 2005; Hansen et al. 2009; Shang et al. 2011). The issue is not limited to the *Herschel* power spectrum since similar conclusions can also be reached with fits to the Planck CFIRB power spectrum. Prior to *Herschel*, the low signal-to-noise CFIRB power spectrum reported by BLAST (Viero et al. 2009) required a halo profile that extends out to $\sim 4r_{\text{vir}}$ to fit the data, leading to an overestimate of the mean density of dark matter in the universe relative to the value in Ω_m that normalizes the dark matter halo mass function.

While a power-law description of the CFIRB power spectrum out to $\ell \sim 2000$ is likely adequate for the dusty galaxy power spectrum in ground-based arcminute-scale CMB anisotropy data (Addison et al. 2011), a clear departure from the power-law was detected in the *Herschel* measurement out to $\ell > 10^4$, indicating the transition between the 2-halo and 1-halo term of galaxy clustering. A proper description of the *Herschel* CFIRB power spectrum must then move beyond the power-law fit to the data. We also refer the reader to Penin et al. (2012); Bethermin et al. (2012) for more recent modeling of CFIRB, concentrating on the Planck-measured CFIRB power spectrum, and Xia et al. (2012) for modeling of both Planck and *Herschel*.

This paper is organized as follows: in the next Section we outline the *Herschel* data used for this analysis. In Section 3 we present a revised CLF model for the CFIRB anisotropy power spectrum. In Section 4 we present our results and conclude with a summary in Section 5. Throughout this paper we assume the

fiducial cosmology for the Λ CDM model of WMAP-7 results (Komatsu et al. 2011).

2. DATA USED FOR THE ANALYSIS

The CFIRB angular power spectrum used for this analysis is the same as that of Amblard et al. (2011), taken from the *Herschel* Multi-tiered Extra-galactic survey (Oliver et al. 2010) with the Spectral and Photometric Imaging Receiver (Griffin et al. 2010) on-board the *Herschel* Space Observatory (Pilbratt et al. 2010). While the measurements were reported for three wavelengths, we concentrate on the $250 \mu\text{m}$ angular power spectrum since it has the highest signal-to-noise and the best resolution.

The luminosity function data measured by *Herschel* are taken from Vaccari et al. (2010) at low redshifts ($z < 0.2$) at $250 \mu\text{m}$. The high- z luminosity function data extending up to $z = 4$ at $250 \mu\text{m}$ are from Eales et al. (2010) and Lapi et al. (2011). We use data from Eales et al. (2010) in 2 bins at $0.2 < z < 0.4$ and $0.4 < z < 0.8$. These luminosity functions are based out of optical and near-IR photometric or spectroscopic redshifts for $250 \mu\text{m}$ -detected galaxies in the GOODS-North field. To extend the $250 \mu\text{m}$ LFs to higher redshifts we make use of the results from Lapi et al. (2011). These luminosity functions are somewhat uncertain as they are based on the sub-mm photometric redshifts, which for each galaxy could have an error of at least 0.3 in $\Delta z/(1+z)$ (Harris et al. 2012). In any case some of that uncertainty is captured by the errors of the LF. In future with more exact LFs our model can be further improved.

The low- z luminosity function data are shown in Fig. 1 left, while the CFIRB angular power spectrum data are in Fig. 2 left. Fig. 3 left shows the high redshift luminosity functions data.

3. HALO-MODEL AND LUMINOSITY FUNCTION FORMALISM

The CLF model we use here to analyze the LF and $P(k)$ data is largely based on the model of Giavalisco & Dickinson (2001) and Lee et al. (2009). One of the main advantages of this improved description of a halo model is that it clearly connects the luminosity function to clustering of galaxies, allowing to simultaneously constrain the model parameters using both these observables. The connection between 1-point (LF) and 2-point ($w(\theta)$, $P(k)$) is based on an explicit model of the galaxy luminosity-halo mass relation as a function of redshift. When compared to the standard halo model with galaxy statistics described by an occupation number, such a luminosity based approach is capable of accounting for the fact that the luminous galaxies are more likely to be in more massive halos. Moreover, the CLF-based model description of Lee et al. (2009) is general enough to reproduce a wide range of shapes for the galaxy luminosity-halo mass relation and its scatter. This is advantageous as the shape of this relation is expected to be different at far-IR wavelengths when compared to the same data at optical wavelengths.

The fundamental ingredients in this revised CLF model are the mass functions for halos and sub-halos and the galaxy luminosity-halo mass relation and its

evolution. The probability density for a halo or a sub-halo of mass M to host a galaxy with luminosity L is modeled as a normal distribution with

$$P(L|M) = \frac{\eta_{\text{DC}}}{\sqrt{2\pi}\sigma_L(M)} \exp\left[-\frac{(L - \bar{L}(M))^2}{2\sigma_L(M)^2}\right], \quad (1)$$

where η_{DC} is the *duty cycle* factor related to the duration of the star formation in the halos (and is $0 \leq \eta_{\text{DC}} \leq 1$). More precisely, the duty cycle represents a measure of the duration of the star formation, t_{SF} , relative to the time interval probed by the survey or the observations, Δt . As discussed in Lee et al. (2009), the ratio $t_{\text{SF}}/\Delta t$ determines the number of halos that can host a detectable galaxy and is hence related to the ratio between the number densities of galaxies and available halos to host such galaxies n_g/n_h . This is precisely the duty cycle η_{DC} we have introduced above.

Note that this description of the duty cycle is different from the ‘‘duty cycle’’ reported by Shang et al. (2011) for dusty, starforming galaxies in their halo/CLF modeling of the Planck CFIRB power spectra. In their work, the duty cycle is derived by comparing the measured shot-noise amplitude, that dominates anisotropy power spectrum at small angular scales, to a prediction of the expected shot-noise given the number density of halos and the observed counts. Given that the shot-noise is $\int dS S^2 dn/dS$, where S is the flux density and dn/dS is the number counts, the shot-noise quoted in their paper is weighted more towards the bright, rare sources. The model comparison by Shang et al. (2011) suggests a duty cycle that is close to one suggesting that the CFIRB anisotropies are dominated by normal quiescent galaxies. Here we provide a precise estimate of the duty cycle down to a specific luminosity and as a function of redshift.

In eq. 1, $\sigma(M)$ is the scatter in the luminosity-mass relation. In this description the scatter can be related to the nature of the starformation. High values for the scatter with respect to the mean luminosity $\bar{L}(M)$ imply a star formation dominated by starbursts while low values for scatter, suggesting a fixed relation between halo mass and luminosity, are typical of quiescent, steady star formation (see also discussion in Lee et al. 2009).

The relation between the halo mass and the average luminosity $\bar{L}(M)$ is expected to be an increasing function of the mass with a characteristic mass scale M_{0l} and we can write (see Lee et al. (2009))

$$\bar{L}(M) = L_0 \left(\frac{M}{M_{0l}}\right)^{\alpha_l} \exp\left[-\left(\frac{M}{M_{0l}}\right)^{-\beta_l}\right], \quad (2)$$

and the scatter can be parameterized in a similar way

$$\sigma(M) = \sigma_0 \left(\frac{M}{M_{0s}}\right)^{\alpha_s} \exp\left[-\left(\frac{M}{M_{0s}}\right)^{-\beta_s}\right]. \quad (3)$$

As already discussed by Lee et al. (2009) these parameterizations don’t have a specific physical motivation (except for the requirement of being increasing function of mass), but offer the advantage to explore a large range of possible shapes. We need to consider the total halo mass function, that is the number

density of halos or sub-halos of mass M . The contribution of halos $n_h(M)$ is taken to be the Sheth & Tormen relation (Sheth & Tormen 1999). The sub-halos term can be modeled through the number of sub-halos of mass m inside a parent halo of mass M_p , $N(m|M_p)$. The total mass function is then

$$n_T(M) = n_h(M) + n_{sh}(M), \quad (4)$$

where $n_{sh}(M)$ is the sub-halo mass function

$$n_{sh}(M) = \int N(M|M_p)n_h(M_p)dM_p. \quad (5)$$

We parameterize $N(m|M)$ as in van de Bosch et al. (2005)

$$N(m|M) = \frac{\gamma}{\beta\Gamma(1 - \alpha_{sh})} \left(\frac{m}{M\beta_{sh}}\right)^{-\alpha_{sh}} \exp\left(-\frac{m}{M\beta_{sh}}\right) \quad (6)$$

where

$$\gamma = \frac{f_{sh}}{\Gamma(1 - \alpha_{sh}, 1/\beta_{sh}) - \Gamma(1 - \alpha_{sh}, 10^{-4}/\beta_{sh})}. \quad (7)$$

Here $\Gamma(x)$ is the incomplete gamma function and f_{sh} is the sub-halo mass fraction. As shown in van de Bosch et al. (2005), where the model is calibrated using numerical simulations, both the normalization and the slope of the sub-halo mass function are not universal and depend on the ratio between the parent halo mass and the non linear mass scale, M_* , defined as the mass scale where the rms of the density field $\sigma(M, z)$ is equal to the critical over-density required for the spherical collapse $\delta_c(z)$. The term f_{sh} in eq. 7 is fitted by the relation

$$\log\{f_{sh}\} = [0.4(\log(M/M_*) + 5)]^{1/2} + 2.74, \quad (8)$$

in numerical simulations and we make use of it in this study.

The best-fit relation for the slope parameters α_{sh} and β_{sh} found by van de Bosch et al. (2005) is

$$\alpha_{sh} = 0.966 - 0.028 \log(M/M_*), \quad (9)$$

and $\beta_{sh} = 0.13$, independent of M . With this description the total number of free parameters in the CLF model is 9 with 4 parameters for the luminosity-mass relation in eq. 2, 4 parameters for the scatter in eq. 3, and the duty cycle parameter η_{DC} .

If the same luminosity-mass relation applies to both halos and sub-halos, then the product $P(L|M)n_T(M)dLdM$ gives the number densities of galaxies with luminosity L in halos or sub-halos of mass M . The luminosity function is then

$$\phi(L)dL = dL \int dM P(L|M)n_T(M). \quad (10)$$

The formalism introduced above also allows us to construct the halo occupation distribution (HOD) in a simple way. The contribution of central galaxies is simply the integration of $P(L|M)$ over all luminosities above a certain threshold L_0 either fixed by the survey or a priori selected so that

$$\langle N_c(M) \rangle_{L \geq L_{min}} = \int_{L_{min}} P(L|M)dL, \quad (11)$$

which, in absence of scatter, reduces to a step function $\Theta(M - M_0)$ as expected. For the satellite galaxies, the HOD is related to the sub-halos

$$\langle N_s(M) \rangle_{L \geq L_{min}} = \int_{L_{min}} dL \int dm N(m|M) P(L|m) \quad (12)$$

The total HOD is then

$$\langle N_{tot}(M) \rangle_{L \geq L_{min}} = \langle N_h(M) \rangle_{L \geq L_{min}} + \langle N_{sh}(M) \rangle_{L \geq L_{min}} \quad (13)$$

The model described so far holds at a given redshift. The duty cycle parameter η_{DC} and the luminosity-mass relation with its scatter are expected to have a redshift evolution. Here we are attempting to fit LF data at a variety of redshift bins between $0 < z < 4$. To account for the redshift evolution of the parameters we assume that the parameters that describe the low redshift ($z < 0.2$) dusty galaxy population are different from those for the high redshift galaxies. Moreover, the high- z data extend from $z = 0.2$ to $z = 4$ and are divided into 6 redshift bins. We thus fit a total of 7 duty cycle parameters, one for each of the bins and do not attempt to constrain the duty cycle variation with a parameterized approach on the redshift evolution. For the evolution of the galaxy 250 μm luminosity-halo mass relation we account for the possible redshift evolution by introducing another parameter, p_M and rewriting the mass scale M_{0l} as

$$M_{0l}(z) = M_{0l,z < 0.2} (1 + z)^{p_M}, \quad (14)$$

where we allow the evolution to follow the assumed power-law form.

Once the HOD is defined, it is possible to calculate the one-halo and two-halo terms of the far-IR anisotropy power spectrum. First, we define the power spectrum in terms of redshift-dependent three-dimensional clustering and will later project them along the line of sight to calculate the angular power spectrum of CFIRB anisotropies. Here we assume that the central galaxy is at the center of the halo and that the halo radial profile of satellite galaxies within dark matter halos follow that of the dark matter given by the Navarro, Frenk and White (NFW) profile (Navarro et al. 1997). The one-halo term is then

$$P^{1h}(k) = \frac{1}{n_g^2} \int dM \langle N_T(N_T - 1) \rangle u(k, M)^p n_h(M) \quad (15)$$

where $u(k, M)$ is the NFW profile in Fourier space and n_g is the galaxy number density

$$n_g = \int dM \langle N_g(M) \rangle n_h(M). \quad (16)$$

The second moment of the HOD that appear in eq. 15 can be simplified as

$$\langle N_T(N_T - 1) \rangle \simeq \langle N_T \rangle^2 - \langle N_h \rangle^2, \quad (17)$$

and the power index p for the NFW profile is $p = 1$ when $\langle N_T(N_T - 1) \rangle < 1$ and $p = 2$ otherwise (Lee et al. 2009). The two-halo term of galaxy power

spectrum is

$$P^{2h}(k) = \left[\frac{1}{n_g} \int dM \langle N_T(M) \rangle u(k, M) n_h(M) b(M) \right]^2 \times P_{lin}(k), \quad (18)$$

where $P_{lin}(k)$ is the linear power spectrum and $b(M)$ is the linear bias factor calculated as in Cooray & Sheth (2002). The total galaxy power spectrum is then $P_g(k) = P^{1h}(k) + P^{2h}(k)$.

As the observations are anisotropies on the sky projected along the line of sight, the observed angular power spectrum can be related to the three-dimensional galaxy power spectrum through a redshift integration along the line of sight (Knox et al. 2001):

$$C_\ell^{\nu\nu'} = \int dz \left(\frac{d\chi}{dz} \right) \left(\frac{a}{\chi} \right)^2 \bar{j}_\nu(z) \bar{j}_{\nu'}(z) P_g(\ell/\chi, z) \quad (20)$$

where χ is the comoving radial distance, a is the scale factor and $\bar{j}_\nu(z)$ is the mean emissivity at the frequency ν and redshift z per comoving unit volume that can be obtained from the LFs as

$$\bar{j}_\nu(z) = \int dL \phi(L, z) \frac{L}{4\pi}. \quad (21)$$

This model does not rely on the assumption of a number counts shape or an evolution. We are able to directly model-fit the mean emissivity as a function of redshift.

α_l	0.22 ± 0.10
β_l	0.70 ± 0.05
$\log(M_{0l}/M_\odot)$	11.5 ± 1.7
$\log(L_0/L_\odot)$	9.6 ± 2.4
$\eta_{DC} (0 < z < 0.2)$	0.54 ± 0.26

TABLE 1
BEST-FIT PARAMETER VALUES AND THEIR $1 - \sigma$ UNCERTAINTIES FROM THE LOW-REDSHIFT LUMINOSITY FUNCTION DATA OF VACCARI ET AL. (2010)

α'_l	0.57 ± 0.03
β'_l	0.19 ± 0.02
$\log(L'_0/L_\odot)$	9.58 ± 0.02
C_{250}	0.78 ± 0.16
$\eta_{DC} (0.2 < z < 0.4)$	0.43 ± 0.07
$\eta_{DC} (0.4 < z < 0.8)$	0.30 ± 0.04
$\eta_{DC} (1.2 < z < 1.6)$	0.16 ± 0.01
$\eta_{DC} (1.6 < z < 2.0)$	0.19 ± 0.01
$\eta_{DC} (2.0 < z < 2.4)$	0.33 ± 0.01
$\eta_{DC} (2.4 < z < 4.0)$	0.31 ± 0.02
p_M	-4.32 ± 0.09

TABLE 2
BEST-FIT PARAMETER VALUES AND THEIR $1 - \sigma$ UNCERTAINTIES FROM THE COMBINATION OF ANGULAR CFIRB POWER SPECTRUM AT 250 μm AND HIGH- z LUMINOSITY FUNCTION DATA.

4. RESULTS AND DISCUSSION

In the revised CLF model outlined above, in principle, we have 23 free parameters: 7 duty cycle parameters, 8 parameters for the luminosity-mass relation and its scatter at low redshifts, 7 parameters for the same relations at high redshifts plus the parameter p_M for the $(1+z)$ redshift evolution of the mass scale (eq. 14).

Separately, the CFIRB power spectrum contains the contribution from Galactic cirrus, in addition to the extragalactic anisotropies traced by the faint, dusty galaxies. In Amblard et al. (2011) the authors accounted for this contamination assuming the same cirrus power-law power-spectrum from measurements of IRAS and MIPS (Lagache et al. 2007) at $100\mu\text{m}$ and extending it to higher wavelengths using the spectral dependence of Schlegel et al. (1998). Such a frequency scaling resulted in an overestimated cirrus correction, as noted by the Planck team (Planck Collaboration, 2011) in their analysis of the CFIRB power spectrum compared to the *Herschel* power spectrum. This is primarily due to the fact that the cirrus is likely overestimated in Schlegel et al. (1998) as IRAS $100\mu\text{m}$ also contains the extragalactic background intensity. To avoid biasing our power spectrum low by an overestimated cirrus correction, we re-fit the raw power spectrum data from Amblard et al. (2011). Here we adopt the same power-law cirrus fluctuation power spectrum used in Amblard et al. (2011), with $P(k) \propto k^{-n}$ with $n = -2.89 \pm 0.22$ as measured by (Lagache et al. 2007). However, we rescale the amplitude of the cirrus power spectrum with a dimensionless factor C_{250} that we keep as a free parameter and model-fit that as part of the global halo model. This implies another free parameter in our model, leading to a total of 24 parameters. Given the large volume of the parameter space, a MCMC analysis (see below) through the full parameter space is very time-consuming. Moreover, it is unlikely that the information carried by the current data is able to constrain such a large number of free parameters.

We hence simplify the analysis as follows. We first fit the low-redshift parameters to the $z < 0.2$ $250\mu\text{m}$ luminosity function measurements from Vaccari et al. (2010) by only varying the 4 parameters related to the luminosity-halo mass relation and the duty cycle at low redshift, $\eta_{\text{DC}}(z < 0.2)$. We assume no scatter in the luminosity-mass relation. When fitting to high redshift data the total number of free parameters is 11: 3 parameters for the $L - M$ relation ($\alpha'_l, \beta'_l, L'_{0l}$, while $M_{0l, z < 0.2}$ is kept fixed to the value found for the $z < 0.2$ LF), plus the power index p_M to account for the evolution of M_{0l} , 6 duty cycle parameters and 1 amplitude for the cirrus contamination, C_{250} . When model fitting to the measured angular power spectrum at $250\mu\text{m}$ we calculate the total theoretical C_ℓ as the sum of the C_ℓ for the low- z HOD found in the previous fit and the C_ℓ calculated at $z > 0.2$. This allows us to treat two types of galaxy populations that are contributing to the *Herschel* galaxy population, the low- z ($z < 0.1$) dust in late-type galaxies and the dusty spheroidal galaxies at high redshifts (Lagache et al. 2003), and to account for a possible

redshift evolution of the others L-M relation parameter (L_0, α_l, β_l). Here we consider galaxies brighter than $L > 5 \times 10^7 L_\odot$ for the low redshift model, while we use $L > 10^9 L_\odot$ to model-fit the high redshift data. These values are consistent with the flux cut of the galaxy samples considered. In order to account for the uncertainty in the exact value of L_{min} we have verified that an order of magnitude change in the value of L_{min} leads to changes in the power spectra of the order of 5 to 6% which is comparable to the 1σ error bars of the data. We find that the exact value of L_{min} , within an order of magnitude, does not change the results considerably.

To model-fit the data we implement a Markov Chain Monte Carlo (MCMC) analysis using a modified version of the *cosmoMC* Lewis & Bridle (2002) package. The results for the low- z $z < 0.2$ $250\mu\text{m}$ luminosity function data are shown in Fig. 1 and in Table 1, where we show and tabulate the best-fit to the luminosity function data and the best-fit values for the CLF parameters involved with the LF description, respectively. In Fig. 1 we show the HOD calculated for the best-fit values of the parameters and its uncertainties.

The best-fit model to the angular power spectrum data and high- z luminosity functions is shown in Figures 2-3. In Table 2 we tabulate the best-fit parameter values (where the prime is used to distinguish the parameters for the high- z luminosity-mass relation from those for the low- z case) and in Fig. 4 we show the probability contours for the luminosity-mass relation parameters.

These results show that the model is able to fit the data even assuming no scatter in the luminosity mass relation. The HOD shows a sharp cut-off at a mass of about $\log(M_{\text{min}}/M_\odot) \simeq 10.8$ at $z = 0$. This quantity could be compared to the threshold mass of the standard halo model and it is in agreement with the results of Amblard et al. (2011), where it was found that $\log(M_{\text{min}}/M_\odot) \simeq 11.5$ with a simple HOD for the dusty galaxies. However it should be noted that in this work we are not fitting directly the value of M_{min} as it is not a free parameter in our model. Thus a direct comparison of our work to Amblard et al. (2011) may not be appropriate.

Both the values mentioned above are different from the recent results of Shang et al. (2011), where the authors used an improved version of the halo model including a luminosity-mass relation to analyze the Planck-based CFIRB anisotropy power spectrum (Planck Collaboration, 2011). They found that the most efficient halo mass scale for starformation is $M_{\text{eff}} \simeq 10^{12.65} M_\odot$, which is closer to the typical value of optical galaxies in the standard halo model (Cooray & Sheth 2002; Abazajian et al. 2005). Nevertheless, again, as already noted in Shang et al. (2011), the model used there is different from the one used in Amblard et al. (2011) (and from the one used in this paper), and a direct comparison between M_{eff} and M_{min} may not be accurate. A proper comparison of our model to the results of Shang et al. (2011) can be done through the effective halo mass scale:

$$M_{\text{eff}} = \int dM n_h(M) M \frac{N_T}{ng} , . \quad (22)$$

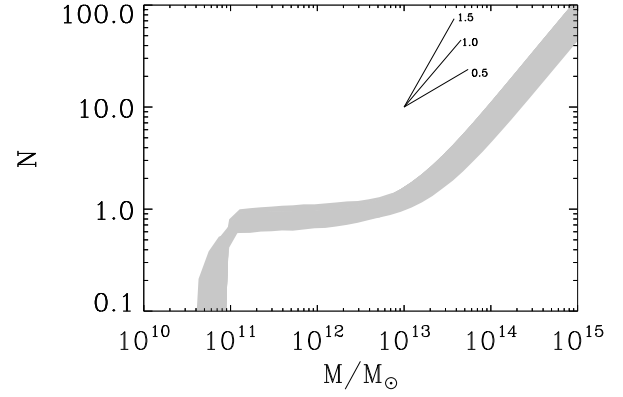
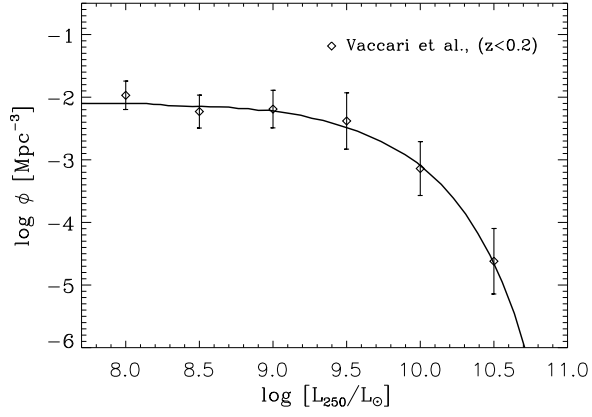


FIG. 1.— *Left*: $250\ \mu\text{m}$ luminosity function data at $z < 0.2$ and the best-fit model. *Right*: The halo occupation number at $z < 0.2$. The minimum halo mass to host a galaxy with luminosity $L > 5 \cdot 10^7 L_\odot$ is $\log(M_{\text{min}}/M_\odot) \simeq 10.8$ and the power-law slope of the satellite galaxies with halo mass is ~ 0.98 . The grey region represents the 68% confidence level and the three lines at the top right of the figure correspond to power-law slopes of 0.5, 1.0 and 1.5.

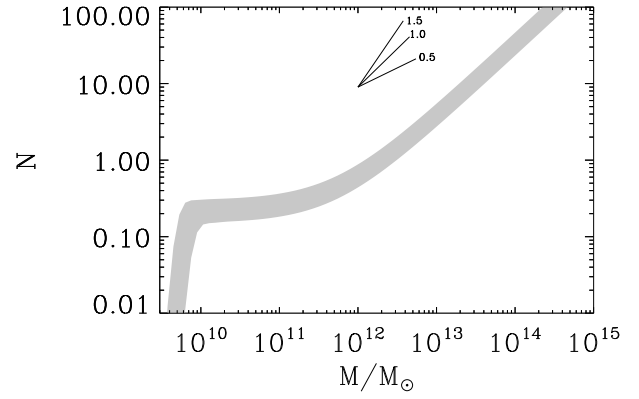
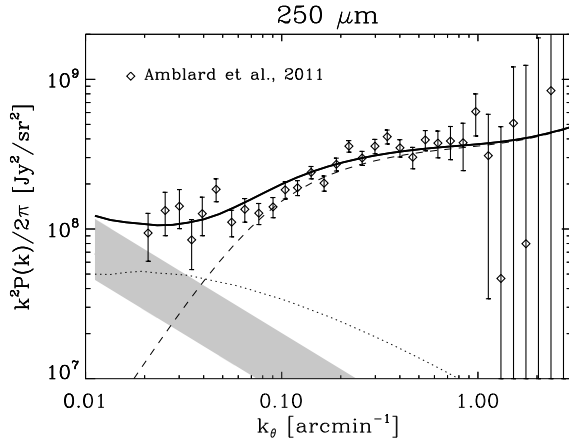


FIG. 2.— *Left*: Best-fit model description to the angular power spectrum data at $250\ \mu\text{m}$. When fitting to the angular power spectrum data we removed the shot-noise contribution as determined by Amblard et al. (2011). Dashed and dotted lines are the 1-halo and 2-halo term, respectively. The shaded region is the 68% confidence level galactic cirrus contribution, as determined by the free parameter C_{250} included in the model-fit. *Right*: The halo occupation number for the high- z galaxies. The HOD slope at the high mass-end is $\simeq 0.96$. The grey region represents 68% confidence level and the three lines correspond to power-law slopes of 0.5, 1.0 and 1.5.

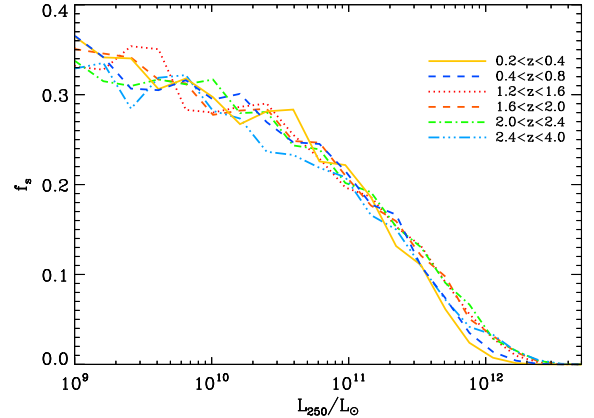
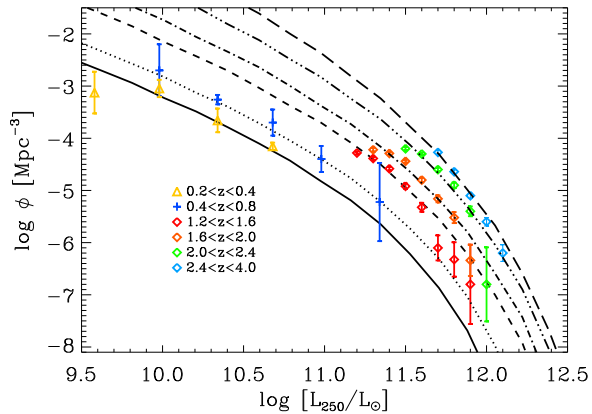


FIG. 3.— *Left*: Best-fit model description to the high-redshift luminosity functions from Eales et al. (2010) and Lapi et al. (2011). *Right*: Satellite fraction at each redshift bin.

Integrating over our HODs, we find $\log_{10}(M_{\text{eff}}) = 12.63$ at $z = 0$, which is comparable to the re-

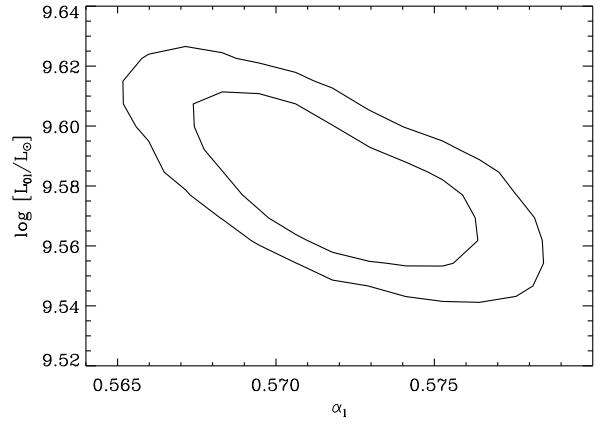
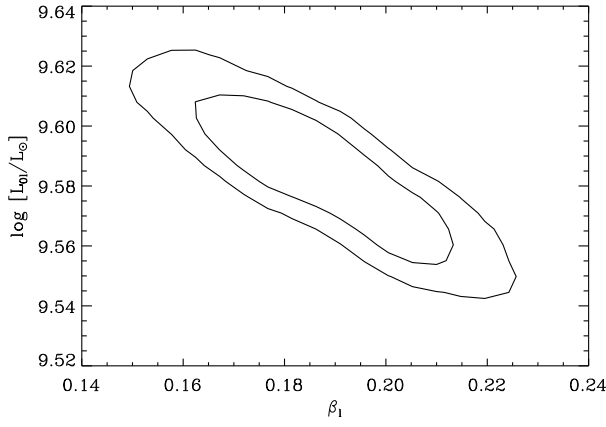


FIG. 4.— 68% and 95% confidence level contours for the parameters of the luminosity-mass relation $L'_0\text{-}\beta'_l$ (left) and $L'_0\text{-}\alpha'_l$ (right).

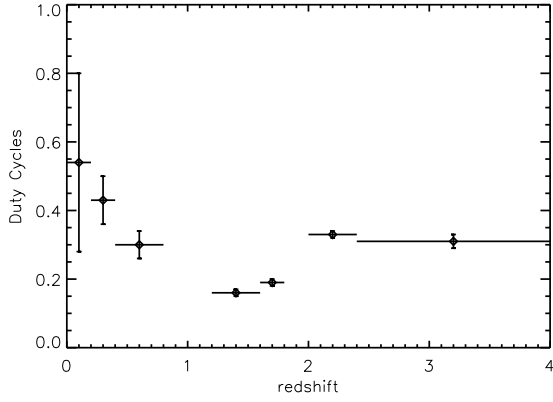


FIG. 5.— Duty cycle η_{DC} as a function of redshift. Over the redshift range of $1 < z < 4$, $\eta_{\text{DC}} \sim 0.2$ to 0.4 .

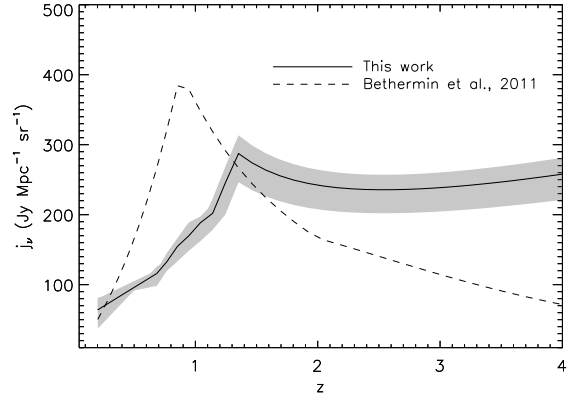


FIG. 7.— $250 \mu\text{m}$ emissivity predicted using the CLF model of this study compared to the model prediction of Bethermin et al. (2011). The shaded region correspond the the 68% confidence level from the MCMC model fits to the measurements used here.

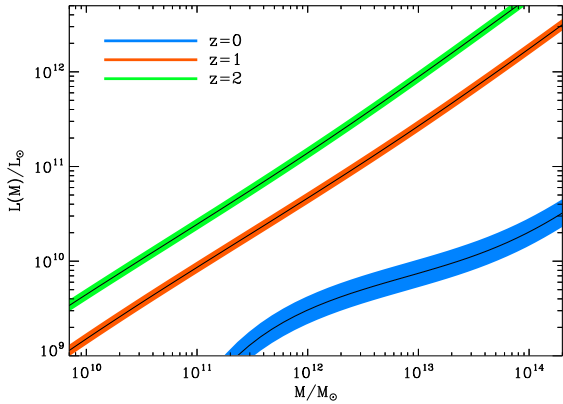


FIG. 6.— The $250 \mu\text{m}$ luminosity-halo mass relation and the 68% confidence level region at $z = 0, 1$ and 2 .

sults of Shang et al. (2011). It is also comparable to results for optical galaxies (Cooray & Sheth 2002; Abazajian et al. 2005). At $z = 1.4$, where the emissivity peaks (see Fig. 7 and discussion below), we find $M_{\text{eff}} = 11.45$.

The contribution of satellite galaxies in our best-fit model becomes efficient at a mass scale $M_{\text{sat}} \simeq 17M_{\text{min}}$ and the HOD of satellite galaxies has a power-law behavior of $\propto M^s$ with the power-law slope

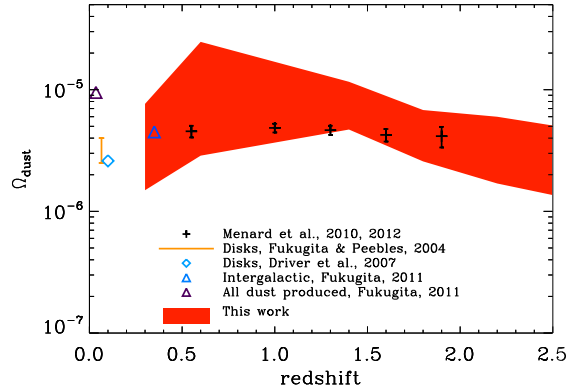


FIG. 8.— The cosmic density of dust Ω_{dust} vs redshift. The CLF model prediction (gray region) calculated with the best-fit luminosity functions of Fig. 3 and compared to other works (see text).

of $s \simeq 0.98$. We show in Fig. 2 that this slope remains close to unity also for the high- z HOD where we find $s \simeq 0.96$. The relation $M_{\text{sat}} \simeq 17M_{\text{min}}$ between minimum halo mass and the halo mass scale at which satellites appears and the slope of the

satellite galaxies occupation number are consistent with expectations from numerical simulations and results obtained for optical galaxies (Gao et al. 2004; Kravtsov et al. 2003; Zheng et al. 2005; Hansen et al. 2009; Shang et al. 2011).

Our result on the power-law slope with $s \sim 0.98$ is different from Amblard et al. (2011) where a higher slope (> 1.6) was found. The difference with $s \sim 1$ and $s > 1.6$ between the two works comes in part from the fact that the model we have presented here accounts for that the brighter satellites are in more massive halos and in part from our rescaling of the cirrus amplitude. As discussed in Planck Collaboration, (2011), Amblard et al. (2011) overestimated the cirrus contamination and underestimates the clustering power spectrum of the cosmic infrared background. We have refitted the cirrus amplitude as part of the joint fit to the power spectrum measurements using both a halo model and a power-law power spectrum for cirrus.

The simple halo occupation number used in Amblard et al. (2011) is not able to make a distinction between the luminosity and mass of satellite galaxies. Moreover, in the current description, the shape of the luminosity-mass relation determines the strength of the 1-halo term, while in the standard halo-model, the strength of the 1-halo term is mainly determined by the slope of the halo occupation number of satellite galaxies. As the 1-halo term is clearly detected in the *Herschel* CFIRB power spectrum the previous results were biased by an incorrect model that attempted to model-fit high signal-to-noise power spectrum measurements. We are also finding an amplitude for the cirrus contamination which is smaller than 1: $C_{250} = 0.78 \pm 0.16$. A reduced cirrus contamination requires a reduced relative amplitude between the 1-halo and 2-halo terms that can be achieved with a lower slope for the satellite contributions. We note also that the fit to the cirrus amplitude confirms that the previous analysis of the same clustering data in Amblard et al. (2011) overestimated the cirrus contribution as already has been found by the Planck Collaboration, (2011), where a factor ~ 2 of difference was found in the cirrus contamination. The model used in this work is hence able to alleviate the tension between Planck and *Herschel* analysis.

In terms of the duty cycle parameters, at $z < 0.2$, where the constrain came only from the luminosity function data, we found a weak constraint on the duty cycle, that is $DC = 0.54 \pm 0.48$ at 95% confidence level. The amplitude of the luminosity function is in fact affected by both the duty cycle and other parameters of the luminosity mass relation, in particular L_0 and M_{0l} . Thus, in the absence of other constraints, the duty cycle can not be measured efficiently. On the other hand, the parameters of the $L - M$ relation also determine the HOD and the relative amplitude of 1-halo and 2-halo terms. Combining clustering measurements and luminosity function data can hence strongly improve the constraints on the duty cycle. Also the $z < 0.2$ luminosity function is better determined in narrow, deeper surveys compared to the case of the $z < 0.2$ LF. All this results

in a determination of high- z duty cycle parameters with relatively small uncertainties. We have found that the duty cycle generally decrease with redshift until $z \simeq 1$ and slowly increase again for higher z (see table 2 and Fig. 5). The values are in the range $\eta_{DC} \simeq 0.16 - 0.4$ when $0.2 < z < 0.4$.

In Shang et al. (2011) the authors have excluded very low duty cycle values ($\eta_{DC} < 0.05$) finding that the Planck power spectrum data favor duty cycles close to unity. Our results lie in the middle between these two extreme cases. However in Shang et al. (2011) the duty cycle parameter is estimated by comparing the shot noise predicted for a fixed η_{DC} to the results of the empirical model of Bethermin et al. (2011), rather than fitting to the data. Moreover the model used here differs in the description of the luminosity mass-relation and introduces a possible redshift evolution both for the duty cycle and for the 250 μm luminosity-halo mass relation. Interestingly our constraints are much more similar to the results of Lee et al. (2009), where the model we are using here, with some differences in the L-M relation and its redshift dependence, was also used to analyze the UV luminosity function and two point correlation function data of starforming galaxies in the range $z = 4 - 6$. In that work Lee et al. (2009) used η_{DC} as an input parameter rather than as a free parameters and found that extremely short ($\eta_{DC} < 0.1$) and extremely long ($\eta_{DC} > 0.7$) duty cycles are ruled out at the 90% confidence level. Our results also suggest a mid range for η_{DC} . The agreement could imply that a large fraction of the UV-selected starforming galaxy sample studied in Lee et al. (2009) could also be responsible for the CFIRB anisotropies. This could be directly tested via a cross-correlation between the two datasets and such studies are expected in the near future given the *Herschel* imaging of some of the wide area legacy fields.

In Section 3 we described the duty cycle in terms of the duration of the starformation t_{SF} in the halos with respect to the time interval Δt covered by the survey. A long duty cycle $\eta_{DC} \sim 1$ implies a starformation time scale that is $t_{SF} \gg \Delta t$, while small duty cycles with $\eta_{DC} \sim 0$ correspond to the opposite case with $t_{SF} \ll \Delta t$. The central value with $\eta_{DC} \sim 0.5$ implies $t_{SF} \simeq \Delta t$. In terms of the physical time, once accounted for the time interval spanned by each redshift bin, the duty cycles listed in Table 2 correspond to a starformation phase lasting for $t_{SF} \simeq 0.3 - 1.6$ Gyr. Such a long starformation timescale is consistent with what has been suggested in Lapi et al. (2011) and the physical model of Granato et al. (2001, 2004). Such a long time scale rule out models where the CFIRB is dominated by gas-rich mergers with $t_{SF} \simeq 10 - 100$ Myr.

It is worth noticing that in this analysis we are assuming a duty cycle that is independent of mass. It could very well be that the duration of starformation depends on the halo mass. Given the large number of free parameters in the analysis we are not able to parametrize a possible mass or luminosity dependence of η_{DC} , but we regard this possibility as a future improvement to this model.

Our analysis suggests that the L-M relation has

a redshift dependence, with M_{0l} that decreases for higher redshifts (see eq. 14). Decreasing M_{0l} is equivalent to increase the characteristic luminosity of the luminosity function. The fit to the high- z luminosity function data is shown in Fig. 3. In particular we find $M_{0l} \propto (1+z)^{-4.32 \pm 0.09}$. Although a direct comparison is complicated because of the very different models used, we note that this result is similar to the evolution seen in LeFloc'h et al. (2005), where the characteristic luminosity has been found to have a redshift dependence $\propto (1+z)^{3.2^{+0.7}_{-0.2}}$.

The total luminosity-mass relation calculated as:

$$L(M) = \bar{L}(M) + \int N(m|M)\bar{L}(m)dM, \quad (23)$$

is shown in Figure 6. The shaded regions represent the 1σ uncertainty and it can be seen that the data are able to constrain the luminosity-mass relation with good precision even for the $z < 0.2$ case using only the low redshift luminosity function data. The luminosity-mass relations we are finding show a linear behavior. However the luminosity functions are steep at the low-faint luminosity end. This result in a tension when the observed turnover is attempted to be explained through the abundance matching approach in Bethermin et al. (2012). We consider this a natural consequence of the fact that in this work we are attempting to fit simultaneously datasets in a large range of redshifts together with anisotropy power spectrum measurements. Moreover we observe that there is no clear visible turnover in the data that we are fitting without imposing any prior or constraint on the faint-end of the luminosity functions. The faint-end description, both in data and in models, should be further improved.

In Figure 7 we show the emissivity corresponding to the best-fit model, calculated according to equation (21) and compared to the emissivity of the parametric model of Bethermin et al. (2011) (see also Penin et al. 2012). The extended tail at $z > 3$ is due to the constant and the fast increase of the luminosity function with redshift. We have verified that using the emissivity of Bethermin et al. (2011) implies a few percent difference in the best-fit values of the CLF parameters in the model presented here, comparable to the 1σ error bars. Future analysis may require however a different redshift parameterization of the average luminosity-mass relation.

We show also the satellite fraction for the four high redshift bins calculated as van de Bosch et al. (2006):

$$f_{sat}(L) = \frac{1}{\phi(L)} \int_{M'}^{\infty} dM P(L|M) n_T(M), \quad (24)$$

where M' is the mass scale where there is one galaxy brighter than L . The satellite fraction is an important test for galaxy formation models and to establish the properties of galaxy-halo relation. We find that the fraction is about 22 – 25% at $L = 10^9 L_{\odot}$ and decreases quickly to less than 5% at $10^{11} L_{\odot}$ while we don't find a significant redshift dependence. The decreasing behavior with mass is due to the fact that satellite galaxies at a given luminosity are located in

more massive (and hence less numerous) halos with respect to central galaxies. This result for f_{sat} is also in agreement with van de Bosch et al. (2006); Cooray (2006b); Coupon et al. (2011).

Finally in Fig. 8 we show the fraction of dust with respect to the critical density of the Universe ρ , calculated as

$$\Omega_{dust} = \frac{1}{\rho_0} \int_{L_{min}} dL \phi(L, z) M_{dust}(L), \quad (25)$$

where M_{dust} is the dust mass corresponding to a given IR luminosity and we use Eq. 4 in Fu et al. (2012). The results are compared to those in Fig. 7 of Menard & Fukugita, (2012) where Ω_{dust} has been determined with reddening of metal-line absorbers. In Fig. 8 we also show other estimates of the mass density of dust as summarized by Menard & Fukugita, (2012) from Fukugita et al. (2004); Driver et al. (2007); Menard et al. (2010); Fukugita (2011). We have combined the points from Menard et al. (2010) for the dust contributions of halos and those from Menard & Fukugita, (2012) in a single set of data points, under the assumption that the amount of dust in halos doesn't evolve significantly with redshift. We parameterize the opacity with a power law $k_d \propto \nu^{\beta_d}$ with the power index in the range $\beta_d = 1.5 - 2$. The calculation requires the spectral energy distribution of dust and we assume a thermal black-body spectrum with dust temperature in the range $T = 25 - 35K$. We allow for a large range in dust temperature, taken as a uniform prior, to allow for the range of values seen in current data (Amblard et al. 2010). In equation (25) we integrate over luminosities $L_{min} > 10^9 L_{\odot}$. However in this calculation the choice of L_{min} is less relevant, since the uncertainty on Ω_{dust} is dominated by the large range of temperatures and spectral indices considered. The gray region correspond to the prediction for these parameters ranges using the best-fit luminosity functions of Fig. 3.

5. CONCLUSION

We have presented an analysis of the *Herschel*-SPIRE CFIRB power spectrum at $250 \mu m$ and the luminosity functions up to $z = 4$. We use a conditional luminosity function approach to model the far-IR bright galaxies. We have modeled the $250 \mu m$ luminosity function and its evolution with redshift introducing a redshift dependent duty-cycle parameter. This description represents an improved version of the halo-model that offers an advantage by accounting for the luminosity dependence of the satellite galaxies as a function of the halo mass. The underlying ingredient is the galaxy luminosity-halo mass relation.

We have found that current *Herschel* data are able to constrain the model despite the high number of free parameters. The results of our analysis indicate that the cosmic far-IR background is dominated by star-forming galaxies in an extended phase of starformation rather than bright starbursts that are fueled by gas-rich mergers. We found duty cycles corresponding to a dusty starformation phase lasting $\sim 0.3 - 1.6$ Gyr, which is in agreement with previous analysis of starforming UV-selected galaxies at high redshifts.

We have also found that the halo occupation number for satellite galaxies has a power-law slope that is about 0.98 over the redshift range $0 < z < 4$. This solves the tension between previous analysis of the same *Herschel* power spectrum data and other determinations of the halo occupation number for galaxies in the literature. Finally we have estimated the cosmic density of dust residing in the dusty, starforming galaxies responsible for the cosmic far-IR background

anisotropies to be $\Omega_{\text{dust}} \sim 3 \times 10^{-6}$ to 2×10^{-5} .

6. ACKNOWLEDGMENTS

We thank Alexandre Amblard for useful communications and Brice Menard for clarifying the SDSS dust measurements. We acknowledge support from NSF CAREER AST-0645427, Herschel funding from NASA Herschel Science Center through a contract from JPL/Caltech, and NASA ADAP award NNX10AD42.

REFERENCES

- Abazajian, K., et al. 2005, ApJ, 625, 613
 Planck collaboration, 2011, A&A, 536, A18
 Addison, G.E., et al. 2011, arXiv:1108.4614
 Amblard, A., & Cooray, A. 2007, ApJ, 670, 903
 Amblard, A., Cooray, A., Serra, P., et al. 2010, A&A, 518, L9+
- Amblard, A., et al. 2011, Nature, 470, 510
 Archidiacono, M., et al. 2012 PRD 85, 043015
 Berta, S., et al. 2011, A&A 532, A49
 Bethermin, M., et al. 2011, A&A, 529, A4
 Bethermin, M., Dore, O., Lagache, G. 2012, 537, L5
 van den Bosch F. C., Tormen G., Giocoli C., 2005, MNRAS, 359, 1029
 van den Bosch, F.C., et al. 2007, MNRAS, 376, 841
 Clements, D.L., Dunne, L., Eales, S. 2010, MNRAS, 403, 274
 Cooray, A., Sheth, R.K. 2002, PR, 372, 1
 Cooray, A., & Milosavljevic, M. 2005, ApJ, 627, L89
 Cooray, A. 2006, astro-ph/0601090
 Cooray, A. 2006, MNRAS, 365, 842
 Coupon, J., et al. 2011, arXiv:1107.0616
 Devlin, M.J., et al. 2009, Nature, 458, 737
 Driver, S. P., et al., 2007, MNRAS, 379, 1022
 Dwek, E., et al. 1998, ApJ, 508, 106
 Eales, S., et al. 2010, A&A, 518, L23
 Fukugita, M., Peebles P. J. E., 2004, ApJ, 616, 643
 Fukugita, M., 2011, arXiv, arXiv:1103.4191
 Fixsen, D. J., et al. 1998, ApJ, 508, 123
 Fu, H., et al. 2012, arXiv:1202.1829
 Gao, L., et al. 2004, MNRAS, 355, 819
 Giavalisco, M., & Dickinson, M. 2001, ApJ, 550, 177
 Glenn, J., et al. 2010, MNRAS, 409, 109
 Granato, G., et al. 2001, MNRAS, 324, 757
 Granato, G.L., et al. 2004, ApJ, 600, 580
 Griffin, M.J., et al. 2010, A&A, 518, L3.1
 Haiman, Z., & Knox, L. 2000, ApJ, 530, 124
 Hansen, S.M., et al. 2009, ApJ, 699, 1333
 Harris, A.I., et al. 2012, arXiv:1204.4706
 Knox, L., et al. 2001, ApJ, 550, 7
 Komatsu, E., et al. [WMAP Collaboration] 2011, ApJ, 192,18
 Kravtsov, A. V., et al. 2004, ApJ, 609, 35
 Lagache, G. 2003, MNRAS, 338, 555
 Lagache, G., et al. 2007, ApJ, 665, L89
 Lapi, A., et al. 2011, ApJ, 742, 1
 Lee, K.S., et al. 2009, ApJ, 695, 368
 Le Flo'c'h, E., et al. 2005, ApJ, 632, 169
 Lewis, A. & Bridle, S. 2002, PRD, 66, 103511
 Menard B., Scranton R., Fukugita M., Richards G., 2010, MNRAS, 405, 1025
 Menard, B., & Fukugita, M. 2012, arXiv:1204.1978
 Navarro, J. F., Frenk, C. S., White, S. D. M. 1997, ApJ, 490, 493
 Negrello, M., et al. 2007, MNRAS, 377, 1557
 Oliver, S., et al. 2010, A&A, 518, L21.1
 Penin, A., et al. 2012, A&A, 537, A137
 Pilbratt, G., et al. 2010, A&A, 518, L1.1
 Puget, J.L., Abergel, A., Bernard, J.P., et al. 1996, A&A, 308, L5
 Schlegel, D.J. 1998, ApJ, 500, 525
 Scott, D., & White, M.J. 1999, A&A, 346, 1
 Shang, C., et al. 2011, arXiv:1109.1522
 Sheth, R. K., & Tormen, G. 1999, MNRAS, 308, 119
 Vaccari, M., Marchetti, L., Franceschini, A., et al. 2010, A&A, 518, L20
 Viero, M. P., et al. 2009, ApJ, 707, 1766
 Wang, J., et al. 2011, MNRAS, 413, 1373
 Xia, J.-Q., et al. 2012, MNRAS, 422, 1324
 Yang, X., et al. 2004, MNRAS, 339, 1057.
 Zehavi, I., et al. 2004, ApJ, 608, 16
 Zheng, Z., et al. 2005, ApJ, 633, 791